Geophysical Research Letters

Supporting Information for

Nickel and chromium stable isotopic composition of ureilites: implications for the Earth's core formation and differentiation of the ureilite parent body

Ke Zhu (朱柯)[1,2]*, Jean-Alix Barrat[3,4], Akira Yamaguchi[5], Olivier Rouxel[6], Yoan Germain[6], Jessica Langlade[4], and Frederic Moynier[2]

[1]Freie Universität Berlin, Institut für Geologische Wissenschaften, Malteserstr. 74-100, 12249 Berlin, Germany

[2]Université de Paris, Institut de Physique du Globe de Paris, CNRS UMR 7154, 1 rue Jussieu, Paris 75005, France

[3]Institut Universitaire de France

[4]Univ Brest, CNRS, IRD, Ifremer, LEMAR, F-29280 Plouzané, France

[5]National Institute of Polar Research, 10-3 Midori-cho, Tachikawa, Tokyo, 190-8518 Japan

[6]Unité de Géosciences Marines, IFREMER, Z.I. Pointe du diable, BP 70-29280 Plouzané, France

*Corresponding Author: Ke Zhu (Email: zhuke618@foxmail.com)

Contents of this file

Introduction

In Supporting Information, we mainly describe the samples and analytical methods and discuss the origin of anomalous Cr stable isotope data for NWA 2236. We also show the figures for elemental mappings of one ureilite, the Ni contents in ureilite metal and bulk samples and the correlation with Fo%, and the 1/[Ni] vs. Ni stable isotope compositions of ureilites. Finally, we reviewed and listed all the Ni stable isotope data for chondrites from literature and this study.

Text S1. Samples and Analytical Methods

For Ni stable isotope compositions, we analyzed 22 un-brecciated ureilites found in Sahara (N = 13) or Antarctica (N = 9), and 3 carbonaceous chondrites (Allende (CV3), Paris (CM2) and Orgueil (CI)). Samples were kindly provided by the NASA meteorite working group (MWG), the National Institute of Polar Research (NIPR), Université de Bretagne Occidentale (UBO), the Museum National d'Histoire Naturelle de Paris and, the Smithsonian Institution (Table 1). Compositions of the olivine cores of the ureilites were previously determined (Barrat et al., 2015 and reference therein), and the bulk compositions of the same samples of chondrites were determined by Barrat et al. (2012) and Hewins et al. (2014). Chemical mapping (Ni, Mg, Fe, S) of a section of a ureilite (NWA 6056) was performed using a Cameca SX100 electron microprobe at service commun "Microsonde Ouest", Plouzané (Figure S1).

Fragments (each of 300–1000 mg) were crushed to a homogeneous fine powder using a boron carbide mortar and pestle. Twenty mg of crushed material was digested by sequential mixtures of HF/HNO_3, HNO_3 and HCl. These procedures allow a perfect dissolution of all the phases except graphite and diamond, which are Ni-free, and have no effect for our study. Aliquots of the solutions were used for the determination of the Ni concentrations by ICP-AES (inductively coupled plasma–atomic emission spectrometry) using a Horiba Jobin Yvon Ultima 2 spectrometer in IUEM, Plouzané.

As for Ni isotope measurements, we employed the double spike technique to correct the potential Ni stable isotope fractionation on column purification and instrumental mass fractionation. Nickel in the dissolved samples was then purified by a two-step ion-exchange chromatography, including the first AG1-X8 resin and second Ni-spec resin (Eichrom). Ni isotopic compositions were determined following the procedure described by Gueguen et al. (2013) and Gueguen and Rouxel (2021), using the Thermo Electron Neptune multi collector–inductively coupled plasma–mass spectrometer (MC-ICP-MS) housed at Ifremer, Plouzané. The reader is referred to the paper by Gueguen et al. (2013) for an extensive description of the procedure. Nickel isotope values are reported relative to the standard NIST SRM 986 using the δ-notation:

$$\delta^{60/58}Ni = (^{60}Ni/^{58}Ni_{sample} / {}^{60}Ni/^{58}Ni_{NIST\ SRM\ 986} - 1) \times 1000 \quad (1).$$

The error associated with sample values is reported as both 2SD and 2SE of the mean (2se) calculated with the 50 cycles of measurements during acquisition on the MC-ICPMS. A sample-standard bracketing method was employed during the analytical protocol, and

thus, replicate measurements of NIST SRM 986 allows the calculation of a two-standard deviation (2SD) as the external error of ~0.05‰. Analyses of USGS certified reference material BHVO-2 measured along with these samples were already published in Gueguen et al. (2013).

As for Cr stable isotope measurements, we used sample aliquots (40%) from Zhu et al. (2020) that includes 11 Sahara main-group ureilites and one ureilitic trachyandesite (Bischoff et al., 2014). To estimate the data quality, we also measured the Cr isotope compositions of the NIST SRM 3112a standard and several USGS geological standard rock powders: BHVO-2 (basalt) and PCC-1 (peridotite). Ten of 11 main-group ureilites overlap with the samples in the Ni isotope list (Table 2). After addition and homogenization of a ^{50}Cr-^{54}Cr double spike (with a spike ratio of ~28%), the purification for Cr is similar than in previous studies (Sossi et al., 2018; Zhu et al., 2021a; Zhu et al., 2021b; Zhu et al., 2019), using a two-step cation-exchange chromatography (Trinquier et al., 2008). The yield is 60% - 90%, and the total Cr blanks are 2-5 ng that is negligible compared to the total 5-20 µg of Cr in the ureilite samples. The final Cr cut was evaporated in concentrated HNO_3 drops, 3 to 5 times, to convert the HCl medium to HNO_3 and to remove leftover organics (i.e., some resin) following which the samples were diluted to a concentration of 1 ppm Cr, in 2% (0.317 M) HNO_3 for isotope analysis.

Neptune Plus MC-ICP-MS, housed at the Institut de Physique du Globe de Paris (IPGP) was used to determine Cr isotope ratios. Analytical details are described in Zhu et al. (2021a), Sossi et al. (2018) and Zhu et al. (2019). The purified sample solution was diluted to ~ 1ppm, which returned a signal of ~ 15V of ^{52}Cr with a Thermo Scientific Stable Introduction System (SIS) with a 50µl/min probe. Every block of measurements is composed of 100 cycles, with integration time of 4.194 s for each cycle. Each sample were measured 2 to 4 times. The final Cr stable isotope data (δ^{53}Cr) for ureilites were corrected using their respective mass–independent Cr isotope compositions that had previously been analyzed on the same aliquots (Zhu et al., 2020). The isotopic ratio for samples is reported in delta notation relative to NIST SRM 979:

$$\delta^{53}Cr(‰) = \left(\frac{\left(^{53}Cr/^{52}Cr\right)_{sample}}{\left(^{53}Cr/^{52}Cr\right)_{NIST\ SRM\ 979}} - 1\right) \times 1000 \quad (2).$$

The uncertainties quoted are the 2SD of individual sample measurements or the 2SD reproducibility of several NIST SRM 979 measurements in the same analytical session (~0.02 ‰), whichever is the largest. The Cr contents were measured by ICP-MS housed at IPGP, and the 2σ uncertainty is 5 to 10%. (Steele et al., 2012).

The $\delta^{60/58}$Ni values for Allende, Orgueil and BIR-1 are consistent with the literature data (Chernonozhkin et al., 2016; Gall et al., 2017; Klaver et al., 2020; Steele et al., 2012; Wang et al., 2021). Furthermore, our two replicate measurements for Allende (0.23 ± 0.02 ‰ and 0.25 ± 0.02 ‰) are also consistent, indicating the good external reproducibility of our Ni stable isotope data. Similarly, the Cr stable isotope data of standard samples, including NIST SRM 3112a (unpurified), PCC-1 and BHVO-2, also accord with previous studies (Bonnand et al., 2016; Liu et al., 2019; Schoenberg et al., 2016; Sossi et al., 2018; Zhu et al., 2019), confirming the accuracy of the δ^{53}Cr values to the stated uncertainties.

Text S2. Anomalous δ^{53}Cr Value for NWA 2236

NWA 2236 has an anomalous δ^{53}Cr value (0.09 ± 0.02‰) that is higher than all the other ureilites. This is not caused by terrestrial weathering that results in an enrichment in the light Cr isotopes (Frei et al., 2014). Note that NWA 2236 also possesses low Cr content (2600 ppm) and high ^{55}Mn/^{52}Cr ratio of 1.14, relative to other main-group ureilites with ^{55}Mn/^{52}Cr ratios ranging from 0.5 to 0.8 (Zhu et al., 2020). However, this chemical and Cr isotopic difference may not be caused by volatile process. Zn is much more volatile than Cr (Lodders, 2003; Sossi et al., 2019), but the Zn content (216 ppm) and isotope composition for NWA 2236 is normal. NWA 2236 is not very depleted in Zn (that is much more volatile than Cr), compared to other main-group ureilites, with normal δ^{53}Cr values, e.g., NWA 7630 and NWA 7686 have Zn contents ranging from 188 and 236 ppm respectively (Brugier et al., 2019). Additionally, NWA 2236 suffered from only a low degree of shock metamorphism after its formation (Brugier et al., 2019). Alternatively, the distinct Cr stable isotope composition of NWA 2236 results from mantle heterogeneity of UPB, and this much higher δ^{53}Cr value can be caused by some mantle process through kinetic isotope fractionation, e.g., diffusion effect. We should note that NWA 2236 also possesses the highest ε^{54}Cr values among the main group ureilites (all the δ^{53}Cr data have corrected for their mass-independent Cr isotope fractionation, i.e., ε^{53}Cr and ε^{54}Cr values), which is likely reflecting mantle heterogeneity (Zhu et al., 2020).

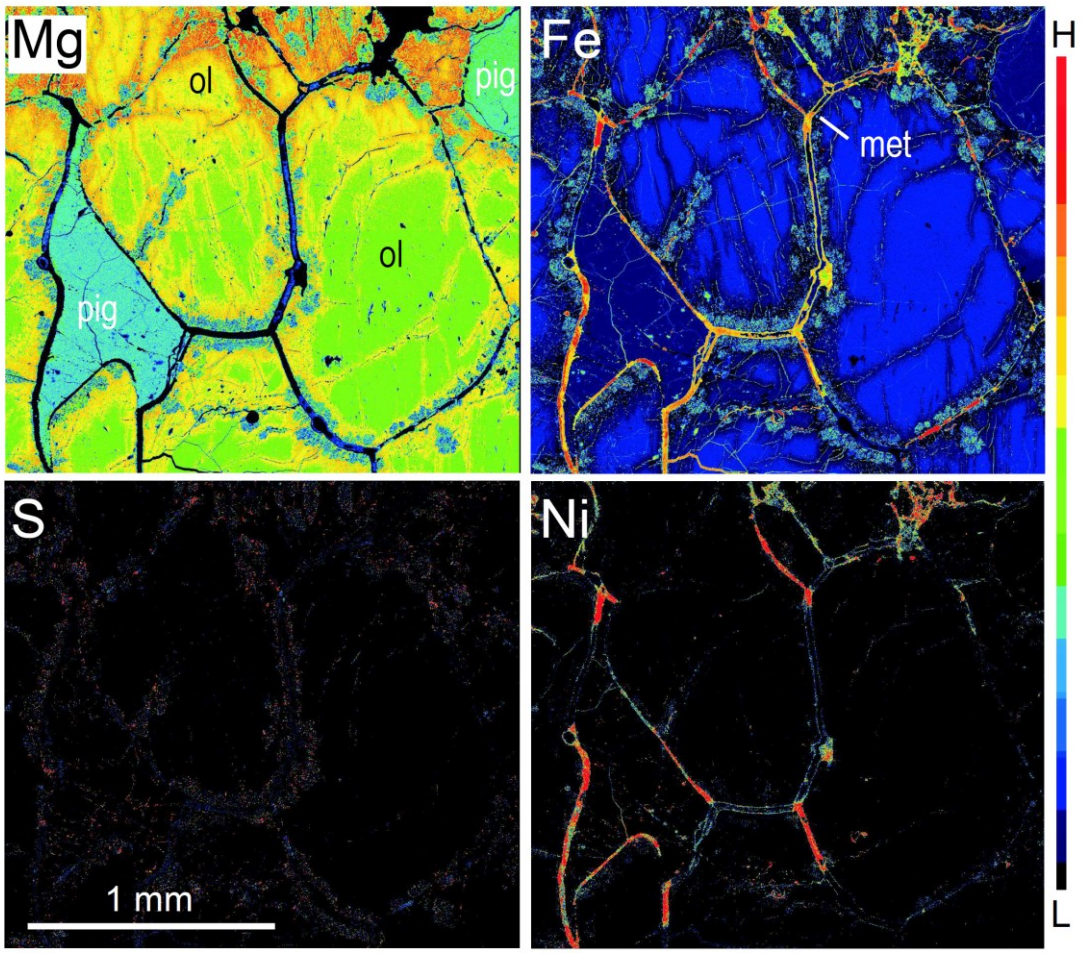

Figure S1. The elemental mapping (Mg, Fe, S and Ni) for NWA 6056. Abbreviation: Olivine-ol; Pigeonite-pig; Metal-met. Ni is mainly residing with Fe and S, and poor in silicate minerals.

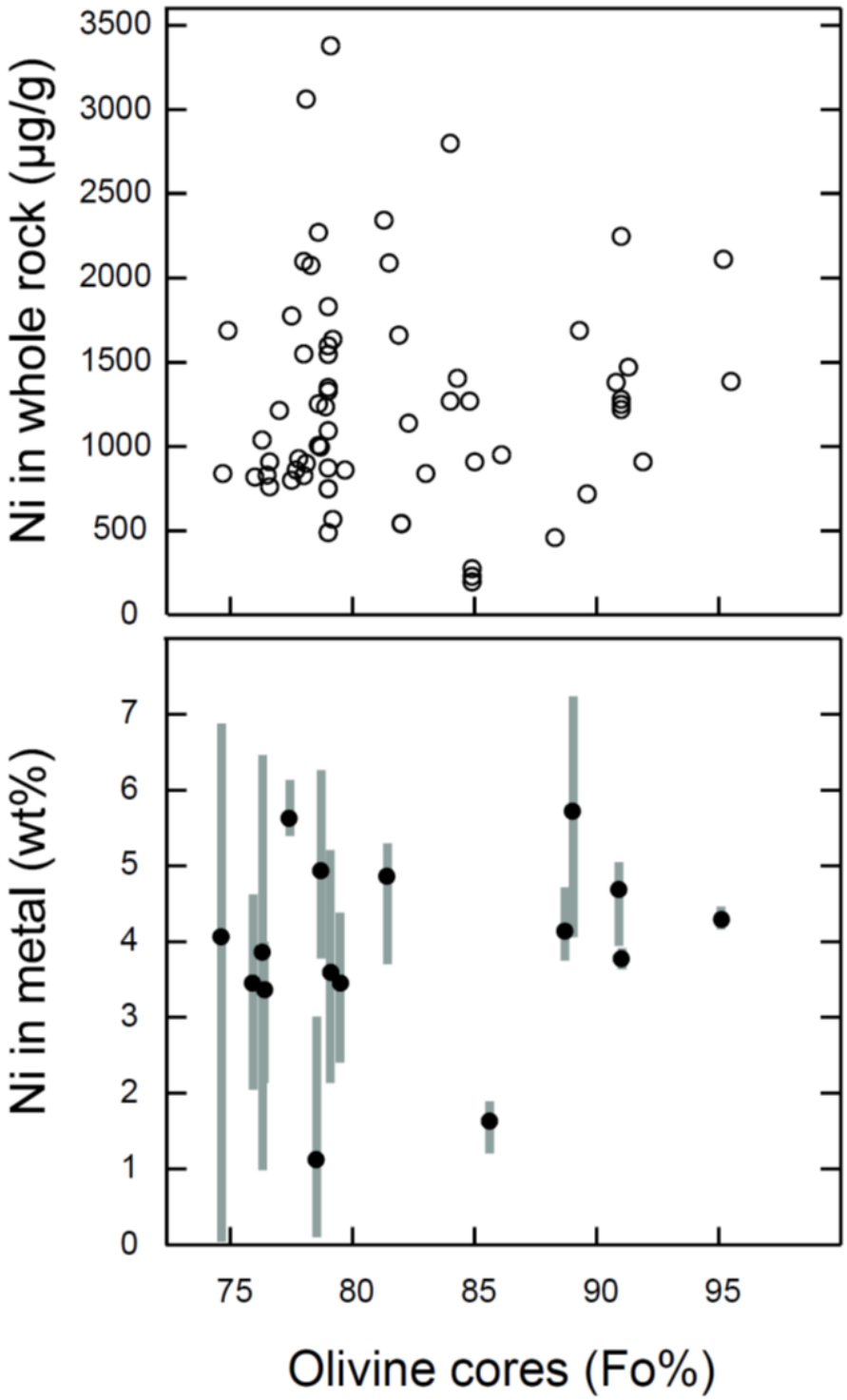

Figure S2 The relationships between Mg# in olivine cores (Fo%) and Ni contents in metals and bulk ureilites (Goodrich et al., 2004; Warren et al., 2006).

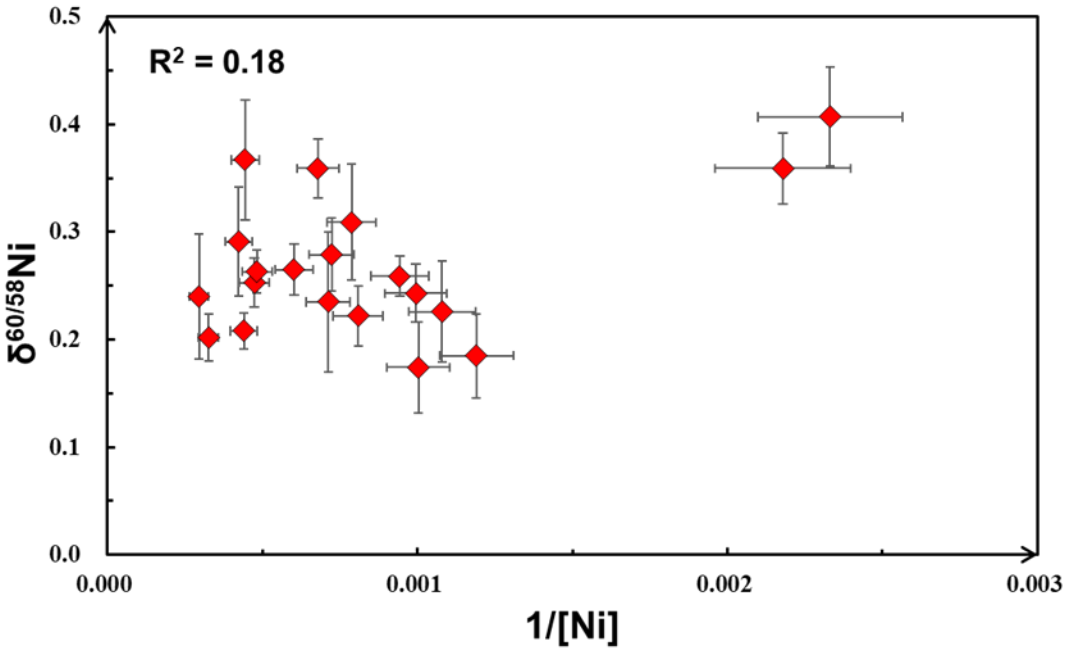

Figure S3 1/[Ni] (Ni contents) versus Ni stable isotope compositions, and there is no clear relationship between them.

Table S1. Review of Ni stable isotope data for chondrites

Sample	Group	$\delta^{60/58}$Ni	2SD	2SE	N	References
Orgueil	CI1	**0.21**	0.07			(Cameron et al., 2009)
Orgueil	CI1	**0.19**		0.024		(Steele et al., 2012)
Orgueil	CI1	**0.18**	0.04		4	(Gall et al., 2017)
Orgueil	CI1	**0.02**	0.02	0.008	8	(Klaver et al., 2020)
Orgueil	CI1	**0.12**	0.02	0.006	8	(Klaver et al., 2020)
Orgueil	CI1	**0.14**	0.05		4	This study
Aver.		**0.14**	0.13			
Ivuna	CI1	**0.11**	0.02	0.006	8	(Klaver et al., 2020)
Murchison	CM2	**0.21**	0.03			(Cameron et al., 2009)
Murchison	CM2	**0.23**	0.07		9	(Gall et al., 2017)
Murchison	CM2	**0.19**	0.03	0.009	8	(Klaver et al., 2020)
Aver.		**0.21**	0.04			
Paris	CM2	**0.23**	0.02		4	This study
Kainsaz	CO3.2	**0.20**	0.03	0.009	8	(Klaver et al., 2020)
Felix	CO3.3	**0.31**	0.07			(Cameron et al., 2009)
Ornans	CO3.4	**0.29**	0.08		9	(Gall et al., 2017)
Ornans	CO3.4	**0.21**	0.02	0.006	8	(Klaver et al., 2020)
Aver.		**0.25**	0.11			
Renazzo	CR2	**0.16**	0.03	0.009	8	(Klaver et al., 2020)
Al Rais	CR2	**0.22**	0.02	0.006	8	(Klaver et al., 2020)
Leoville	CV3.1	**0.30**	0.05			(Cameron et al., 2009)
Kaba	CV3.1	**0.22**	0.04			(Wang et al., 2021)
Allende	CV3.6	**0.24**	0.07		9	(Gall et al., 2017)
Allende	CV3.6	**0.24**	0.03	0.010	8	(Klaver et al., 2020)
Allende	CV3.6	**0.25**	0.04			(Wang et al., 2021)
Allende	CV3.6	**0.23**	0.02		4	
Aver.		**0.25**	0.01			
Karoonda	CK4	**0.28**	0.02	0.008	8	(Klaver et al., 2020)
Karoonda	CK4	**0.39**	0.04			(Wang et al., 2021)
Aver.		**0.33**	0.16			
Kota-kota	EH3	**0.20**	0.03	0.009	8	(Klaver et al., 2020)
Kota-kota	EH3	**0.26**	0.04			(Wang et al., 2021)
Kota-kota	EH3	**0.21**	0.04			(Wang et al., 2021)
Aver.		**0.22**	0.07			
Abee	EH4	**0.19**	0.05			(Cameron et al., 2009)
Abee	EH4	**0.25**	0.02	0.008	7	(Klaver et al., 2020)
Aver.		**0.22**	0.09			

Indarch	EH4	**0.27**	0.09		9	(Gall et al., 2017)
Indarch	EH4	**0.19**	0.03	0.009	8	(Klaver et al., 2020)
Aver.		**0.23**	0.12			
St. Mark's	EH5	**0.18**	0.02	0.006	15	(Klaver et al., 2020)
Khairpur	EL6	**0.29**	0.08		9	(Gall et al., 2017)
Khairpur	EL6	**0.21**	0.02	0.007	11	(Klaver et al., 2020)
Aver.		**0.25**	0.12			
Atlanata	EL6	**0.21**	0.03	0.009	8	(Klaver et al., 2020)
Hvittis	EL6	**0.22**	0.02	0.008	7	(Klaver et al., 2020)
Yilmia	EL6	**0.21**	0.02	0.008	8	(Klaver et al., 2020)
A 10224	L3	**0.24**	0.01		3-5	(Chemonzhkin et al., 2016)
Ceniceros	L3.7	**0.20**	0.03	0.009	8	(Klaver et al., 2020)
Barratta	L4	**0.31**	0.05		9	(Gall et al., 2017)
Barratta	L4	**0.19**	0.03	0.009	8	(Klaver et al., 2020)
Aver.		**0.25**	0.16			
Bruderheim	L6	**0.51**	0.07		5	(Gall et al., 2017)
Chainpur	LL3.4	**0.28**	0.10			(Cameron et al., 2009)
Chainpur	LL3.4	**0.28**	0.04			(Wang et al., 2021)
Aver.		**0.28**	0.00			
Parnalee	LL3.6	**0.20**	0.03	0.009	8	(Klaver et al., 2020)
A 09135	LL3	**0.15**	0.02		3-5	(Chemonzhkin et al., 2016)
Parnalee	LL3	**0.16**	0.05		4	(Gall et al., 2017)
Chelyabinsk	LL5	**0.27**	0.03	0.009	8	(Klaver et al., 2020)
Dhurmsala	LL6	**0.22**	0.02	0.008	8	(Klaver et al., 2020)
Kilabo	LL6	**0.25**	0.03	0.009	8	(Klaver et al., 2020)
St. Severin	LL6	**0.24**	0.05		5	(Gall et al., 2017)
A 09436	H3	**0.20**	0.04		3-5	(Chemonzhkin et al., 2016)
Bremervorde	H3	**0.26**	0.05		5	(Gall et al., 2017)
Buzzard Coulee	H4	**0.17**	0.03	0.009	8	(Klaver et al., 2020)
Kernouve	H6	**0.37**	0.08		4	(Gall et al., 2017)

Note: All chondrites show average $\delta^{60/58}$Ni value of 0.23 ± 0.14 (2SD) ± 0.02 (2SE, N = 37). Literature sources: (Cameron et al., 2009; Chernonozhkin et al., 2016; Gall et al., 2017; Klaver et al., 2020; Steele et al., 2012; Wang et al., 2021)

References

Bischoff, A., M. Horstmann, J.-A. Barrat, M. Chaussidon, A. Pack, D. Herwartz, D. Ward, C. Vollmer, and S. Decker (2014), Trachyandesitic volcanism in the early solar system, *Proceedings of the National Academy of Sciences*, *111*(35), 12689-12692. https://doi.org/10.1073/pnas.1404799111.

Bonnand, P., H. M. Williams, I. J. Parkinson, B. J. Wood, and A. N. Halliday (2016), Stable chromium isotopic composition of meteorites and metal–silicate experiments: Implications for fractionation during core formation, *Earth and Planetary Science Letters*, *435*, 14-21. https://doi.org/10.1016/j.epsl.2015.11.026.

Brugier, Y.-A., J.-A. Barrat, B. Gueguen, A. Agranier, A. Yamaguchi, and A. Bischoff (2019), Zinc isotopic variations in ureilites, *Geochimica et Cosmochimica Acta*, *246*, 450-460. https://doi.org/10.1016/j.gca.2018.12.009.

Cameron, V., D. Vance, C. Archer, and C. H. House (2009), A biomarker based on the stable isotopes of nickel, *Proceedings of the National Academy of Sciences*, *106*(27), 10944-10948. https://doi.org/10.1073/pnas.0900726106.

Chernonozhkin, S. M., S. Goderis, M. Costas-Rodríguez, P. Claeys, and F. Vanhaecke (2016), Effect of parent body evolution on equilibrium and kinetic isotope fractionation: a combined Ni and Fe isotope study of iron and stony-iron meteorites, *Geochimica et Cosmochimica Acta*, *186*, 168-188. https://doi.org/10.1016/j.gca.2016.04.050.

Frei, R., D. Poiré, and K. M. Frei (2014), Weathering on land and transport of chromium to the ocean in a subtropical region (Misiones, NW Argentina): A chromium stable isotope perspective, *Chemical Geology*, *381*, 110-124. https://doi.org/10.1016/j.chemgeo.2014.05.015.

Gall, L., H. M. Williams, A. N. Halliday, and A. C. Kerr (2017), Nickel isotopic composition of the mantle, *Geochimica et Cosmochimica Acta*, *199*, 196-209. https://doi.org/10.1016/j.gca.2016.11.016.

Goodrich, C. A., E. R. Scott, and A. M. Fioretti (2004), Ureilitic breccias: clues to the petrologic structure and impact disruption of the ureilite parent asteroid, *Chemie der Erde-Geochemistry*, *64*(4), 283-327. https://doi.org/10.1016/j.chemer.2004.08.001.

Gueguen, B., and O. Rouxel (2021), The Nickel isotope composition of the authigenic sink and the diagenetic flux in modern oceans, *Chemical Geology*, *563*, 120050. https://doi.org/10.1016/j.chemgeo.2020.120050.

Gueguen, B., O. Rouxel, E. Ponzevera, A. Bekker, and Y. Fouquet (2013), Nickel isotope variations in terrestrial silicate rocks and geological reference materials measured by MC‐ICP‐MS, *Geostandards and Geoanalytical Research*, *37*(3), 297-317. https://doi.org/10.1111/j.1751-908X.2013.00209.x.

Klaver, M., D. A. Ionov, E. Takazawa, and T. Elliott (2020), The non-chondritic Ni isotope composition of Earth's mantle, *Geochimica et Cosmochimica Acta*, *268*, 405-421. https://doi.org/10.1016/j.gca.2019.10.017.

Liu, C. Y., L. J. Xu, C. T. Liu, J. Liu, L. P. Qin, Z. D. Zhang, S. A. Liu, and S. G. Li (2019), High‐Precision Measurement of Stable Cr Isotopes in Geological Reference Materials by a Double‐Spike TIMS Method, *Geostandards and Geoanalytical Research*, *43*(4), 647-661. https://doi.org/10.1111/ggr.12283.

Lodders, K. (2003), Solar system abundances and condensation temperatures of the elements, *The Astrophysical Journal*, *591*(2), 1220-1247. https://doi.org/10.1086/375492.

Schoenberg, R., A. Merdian, C. Holmden, I. C. Kleinhanns, K. Haßler, M. Wille, and E. Reitter (2016), The stable Cr isotopic compositions of chondrites and silicate planetary reservoirs, *Geochimica et Cosmochimica Acta*, *183*, 14-30. http://dx.doi.org/10.1016/j.gca.2016.03.013.
Sossi, P., F. Moynier, and K. van Zuilen (2018), Volatile loss following cooling and accretion of the Moon revealed by chromium isotopes, *Proceedings of the National Academy of Sciences*, *115*(43), 10920-10925. https://doi.org/10.1073/pnas.1809060115.
Sossi, P. A., S. Klemme, H. S. C. O'Neill, J. Berndt, and F. Moynier (2019), Evaporation of moderately volatile elements from silicate melts: experiments and theory, *Geochimica et Cosmochimica Acta*, *260*, 204-231. https://doi.org/10.1016/j.gca.2019.06.021.
Steele, R. C. J., C. D. Coath, M. Regelous, S. Russell, and T. Elliott (2012), Neutron-poor nickel isotope anomalies in meteorites, *The Astrophysical Journal*, *758*(1), 59. https://doi.org/10.1088/0004-637X/758/1/59.
Trinquier, A., J.-L. Birck, and C. J. Allègre (2008), High-precision analysis of chromium isotopes in terrestrial and meteorite samples by thermal ionization mass spectrometry, *Journal of Analytical Atomic Spectrometry*, *23*(12), 1565-1574. https://doi.org/10.1039/B809755K.
Wang, S.-J., et al. (2021), Nickel isotopic evidence for late-stage accretion of Mercury-like differentiated planetary embryos, *Nature Communications*, *12*(1), 294. https://doi.org/10.1038/s41467-020-20525-1.
Warren, P. H., F. Ulff-Møller, H. Huber, and G. W. Kallemeyn (2006), Siderophile geochemistry of ureilites: A record of early stages of planetesimal core formation, *Geochimica et Cosmochimica Acta*, *70*(8), 2104-2126. https://doi.org/10.1016/j.gca.2005.12.026.
Zhu, K., F. Moynier, M. Schiller, C. M. O. D. Alexander, J.-A. Barrat, A. Bischoff, and M. Bizzarro (2021a), Mass–independent and mass–dependent Cr isotopic composition of the Rumuruti (R) chondrites: Implications for their origin and planet formation, *Geochimica et Cosmochimica Acta*, *293*, 598-609. https://doi.org/10.1016/j.gca.2020.10.007.
Zhu, K., F. Moynier, M. Schiller, J. A. Barrat, H. Becker, and M. Bizzarro (2021b), Tracing the origin and core formation of the enstatite achondrite parent bodies using Cr isotopes, *Geochimica et Cosmochimica Acta*, *308*, 256-272. https://doi.org/10.1016/j.gca.2021.05.053.
Zhu, K., F. Moynier, M. Schiller, D. Wielandt, K. Larsen, E. van Kooten, and M. Bizzarro (2020), Chromium isotopic constraints on the origin the ureilite parent body, *The Astrophysical Journal*, *888*, 126. https://doi.org/10.3847/1538-4357/ab5af7.
Zhu, K., P. A. Sossi, J. Siebert, and F. Moynier (2019), Tracking the volatile and magmatic history of Vesta from chromium stable isotope variations in eucrite and diogenite meteorites, *Geochimica et Cosmochimica Acta*, *266*, 598-610. https://doi.org/10.1016/j.gca.2019.07.043.